Journal of Inorganic and General Chemistry
ZAAC
Zeitschrift für anorganische und allgemeine Chemie
doi.org/10.1002/zaac.202100231
ARTICLE

A thorough investigation of the crystal structure of willemite-type Zn_2GeO_4

Joachim Breternitz[+],*[a] Daniel Fritsch[+],*[a] Alexandra Franz,[a] and Susan Schorr*[a, b]

The thermodynamically stable phase of Zn_2GeO_4 contains tetrahedrally coordinated cations only and crystallizes isostructurally to Zn_2SiO_4 (willemite, space group $R\bar{3}$, no. 148). While this material is considered for a plethora of energy-related applications, such as transparent conducting oxide, battery material and photocatalyst, cation ordering in the crystal structure has not been investigated thoroughly. We have therefore re-determined the crystal structure of Zn_2GeO_4 using a combination of X-ray and neutron powder diffraction. The additional neutron diffraction study helps to distinguish between the isoelectronic Zn^{2+} and Ge^{4+} cations and yields valuable information about a partial or complete cation permutation in this material. The experimental study is supported by first-principles calculations on the structural properties of Zn_2GeO_4 utilizing a standard generalized gradient approximation, and the more accurate hybrid functional HSE06. In order to better understand cation permutations, additional calculations including defective Zn_2GeO_4 have been performed based on a supercell approach. Our results show that, with the preparation conditions applied, cation permutation is unlikely to occur in our samples.

Introduction

The structural properties of Zn_2GeO_4 render it useful for a multitude of potential applications. It is currently under investigation as cathode material in Li-ion batteries,[1–3] due to its open structure with large tunnels for potential intercalation (Figure 1). For a possible application as phosphor material in flat panel displays, Zn_2GeO_4 exhibits fairly strong luminescence that is exceeding that of commercial ZnO phosphor by 40%.[4] This strong luminescence is attributed to complex defect behavior of the material when produced via particular processes,[4,5] and can be further enhanced by doping with photoactive ions.[6–8] The susceptibility for photo-activation also qualifies the material as potential photocatalyst system,[9,10] and last but not least, the fact that the material has a very small thermal expansion that is, in fact, negative at lower temperatures has also attracted some interest.[11,12]

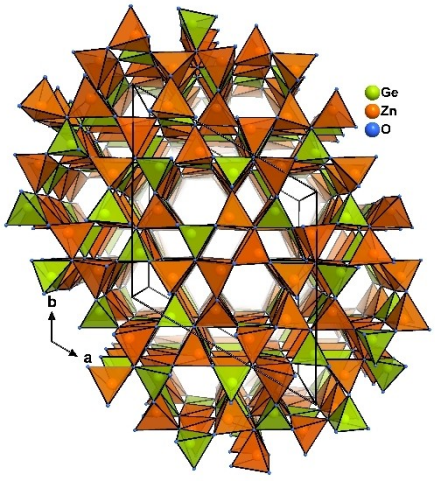

Figure 1. Representation of the crystal structure of Zn_2GeO_4 in central perspective along the crystallographic c-axis. The atoms (Ge: green, Zn: orange, O: blue) are shown as generic balls and the tetrahedra are colored according to the respective central atom.

Further to its inherent properties and potential uses, Zn_2GeO_4 is being used as precursor material for the synthesis of ternary nitride[13] and oxide nitride materials[14–16] that are currently under investigation for photovoltaic[17,18] and photoelectrochemical applications.[19] The crystal structure of Zn_2GeO_4 at ambient conditions is isostructural to Zn_2SiO_4 (willemite, space group $R\bar{3}$, no. 148),[20,21] which itself belongs to the phenacite group and is hence a nesosilicate.[22–24] Interestingly, all constituent atoms occupy a general Wyckoff position 18f, with one for Ge cations (Ge1 in the following), two for the Zn

[a] *Dr. J. Breternitz,[+] Dr. D. Fritsch,[+] Dr. A. Franz, Prof. S. Schorr*
Structure and Dynamics of Energy Materials
Helmholtz-Zentrum Berlin für Materialien und Energie
Hahn-Meitner-Platz 1, 14109 Berlin, Germany
E-mail: Joachim.Breternitz@helmholtz-berlin.de
Daniel.Fritsch@helmholtz-berlin.de
Susan.Schorr@helmholtz-berlin.de
[b] *Prof. S. Schorr*
Department Geosciences
Freie Universität Berlin
Malteserstraße 74–100, 12249 Berlin, Germany
[+] *These authors contributed equally to this work.*

Supporting information for this article is available on the WWW under https://doi.org/10.1002/zaac.202100231

cations (Zn1, Zn2), and four for the O anions (O1 to O4), respectively.

At higher temperatures and pressures, Zn_2GeO_4 also adopts a spinel-type structure,[25] where two thirds of the cation positions switch from tetrahedral to octahedral coordination. Despite the notable interest in this compound, and in particular in its structural and defect behavior, it is surprising that, to the best of our knowledge, no comprehensive neutron diffraction study has been conducted. Such a study is, however, very valuable since Zn^{2+} and Ge^{4+} are isoelectronic and hence virtually indistinguishable by X-ray diffraction and a partial or even complete permutation of the cations on the three independent crystallographic sites (Ge1, Zn1, and Zn2) would easily go unnoticed. The inorganic crystal structure database contains only two crystal structure refinements for the pure Zn_2GeO_4, namely collection codes 16173[20] and 68382,[21] and a more recent one on Tb^{3+} doped Zn_2GeO_4, namely collection code 259671,[26] respectively. There are however, some other crystal structure refinements available, e.g., from Yang et al.[27] and Cheng et al.[12]

In order to advance our current knowledge, we applied a combination of X-ray and neutron diffraction techniques in order to re-determine the crystal structure of Zn_2GeO_4, and supplemented the experimental results with first-principles calculations based on density functional theory (DFT). The combined efforts brought about a more comprehensive understanding of the structural features present in Zn_2GeO_4 and provided an insight on the effects behind the observed features of the material.

Results and Discussion

X-ray Diffraction

Zn_2GeO_4 crystallizes in the rhombohedral space group $R\bar{3}$ with $Z=18$ (in hexagonal setting). Using LaB_6 as internal standard during the measurement allows to determine the lattice constants with high accuracy as $a=14.2351(1)$ Å and $c=9.5280(1)$ Å (in hexagonal setting). These lattice parameters are slightly smaller than the values obtained before ($a=14.284(1)$ Å, $c=9.547(1)$ Å) by single crystal diffraction (compare Table 1 for a more comprehensive overview).[21] It should be noted that powder X-ray diffraction is commonly regarded as the more accurate technique for the determination of lattice parameters, especially when measured with an internal standard as done in this study. The unavoidable zero error in X-rays was corrected using LaB_6 as internal standard in the X-ray diffraction measurement. Further, a small portion of ZnO was found during the refinement but its refined volume fraction is below 2 vol.-%, both in the X-ray and neutron diffraction data. Two constraints were introduced during the refinement: the two crystallographically independent Zn positions (Zn1 and Zn2) were constrained to have identical displacement parameters, and so were the oxygen displacement parameters (O1 to O4). This treatment is necessary, since all seven crystallographically independent atoms are lying on the general 18f Wyckoff position and hence a total of 21 atom position parameters is varied during the refinement. This is also the reason, why the displacement parameters were refined isotropically (one parameter per atom) rather than anisotropically (six parameters per atom). This treatment led to an acceptable fit in the Rietveld refinement (Figure 2) and the results of the analysis of XRD data are summarized in the supplementary information, Tables S1–S3.

Table 1. Lattice parameters determined by Rietveld refinement of the XRD data compared to reported values and those of the DFT optimizations.

method	hexagonal setting		rhombohedral setting		R_p
	a/Å	c/Å	a/Å	α/°	
XRD	14.2351(1)	9.8280(1)	8.811(1)	107.764(2)	0.042
XRD [20]	14.269	9.559	8.836	107.700	0.133
XRD [21]	14.284	9.547	8.840	107.794	0.041
XRD [27]	14.201	9.507			0.010
XRD [12]			8.81	107.7	0.084
PBE	14.482	9.665	8.960	107.823	
HSE06	14.324	9.564	8.863	107.813	

The Ge–O bonding distances are generally shorter than the Zn–O distances and range between $1.74(1)\text{ Å} \leq d_{Ge\text{-}O} \leq 1.857(8)$ Å, while the latter tend to be longer with values between $1.833(9)\text{ Å} \leq d_{Zn\text{-}O} \leq 2.03(2)$ Å. This is consistent with the different Shannon ionic radii of Ge^{4+} (0.4 Å) and Zn^{2+} (0.6 Å)[28] in tetrahedral coordination and coincides excellently with the sum of radii $r_{Ge}+r_O=1.8$ Å and $r_{Zn}+r_O=2.0$ Å. This does, nonetheless, not rule out that the two atom types are at least partially disordered, despite a predicted higher total energy for such defects.

It should be noted that not only the M–O distances scatter, but also the O–M–O angles are spread around the ideal tetrahedral angle (109.5°), ranging from 101.4(5)° to 117.0(5)°. Further, the oxygen atoms are surrounded in a nearly trigonal

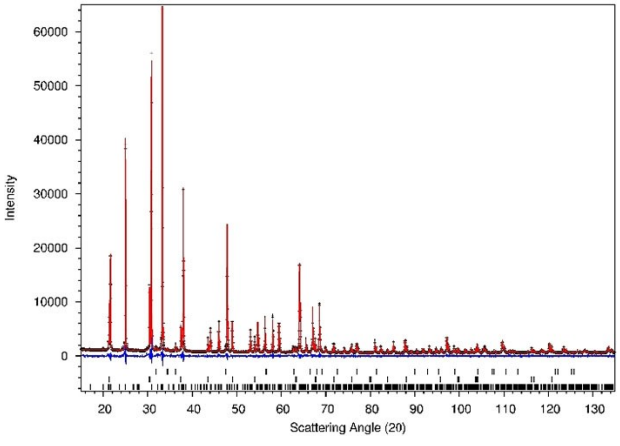

Figure 2. Observed (black crosses) and refined (red line) X-ray powder diffraction profile and their difference (blue line) together with the calculated peak positions (black ticks, bottom to top) for Zn_2GeO_4, LaB_6 (standard) and ZnO.

planar coordination with angles around the ideal 120° from 109.1(5)° to 126.4(7)°.

The structure contains three crystallographically independent tetrahedra that are forming a three-dimensional network through shared corners. Two of these tetrahedra are occupied by Zn and one is occupied by Ge in order to fulfil the stoichiometry of the compound. In analogy to the nesosilicates[29] the Ge containing tetrahedra are uniquely surrounded by Zn-tetrahedra and every oxygen atom is therefore connected to one Ge atom and two Zn atoms. This arrangement is the only possible one for a Pauling rule preserving coordination at the oxygen positions. If Ge and Zn atoms should be distorted, this would result in a local violation of this rule and hence a higher total energy. In order to test for potential antisite defects, X-ray diffraction is not sufficient as Ge^{4+} and Zn^{2+} are isoelectronic and therefore differ only very little in their scattering factors.

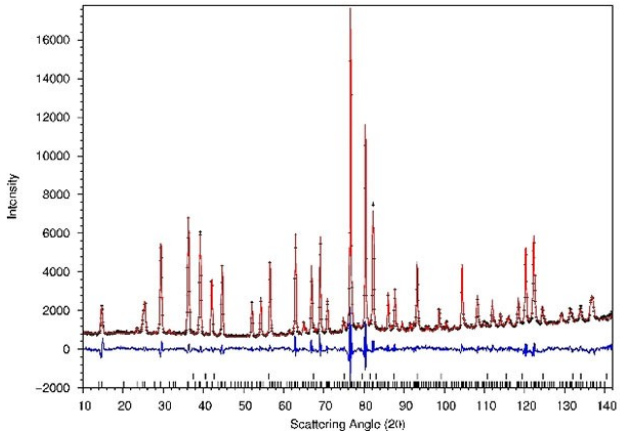

Figure 3. Observed (black crosses) and refined (red line) neutron powder diffraction profile and their difference (blue line) together with the calculated peak positions (black ticks, bottom to top) for Zn_2GeO_4 and ZnO.

Neutron Diffraction

The neutron scattering lengths of Zn (b = 5.680 fm) and Ge (b = 8.185 fm)[30] are, however, sufficiently different for a reliable attribution of the cation sites to the atom types. Given the larger instrumental broadening of the reflections at the neutron diffraction instrument and the less determination of the sample position, we used the lattice parameters obtained from X-ray diffraction in the neutron refinement and only varied zero-point and position error. Due to the fact that the scattering power of oxygen is greatly enhanced in neutron diffraction relative to X-ray diffraction, it was no longer necessary to restrict the displacement parameters for these, but a reliable value for each isotropic displacement could be obtained in the Rietveld refinement (Figure 3; Full details of the neutron refinement are given in the supplementary information, Tables S4–S6). While the cation positions are in close agreement between the refinements of X-ray and neutron diffraction data, the oxygen positions differ more significantly (Table 2). This is also an effect of the larger relative scattering power in neutron diffraction and it is expected that the positions from neutron diffraction are more accurate. Furthermore, the occupancies of the cations on the three crystallographically independent sites were refined

Table 2. Comparison of the atom positions refined from X-ray diffraction and obtained from PBE and HSE06 calculations with respect to the atomic positions refined from neutron diffraction. The differences u_x, u_y and u_z are given in relative units. $||u||$ is the absolute distance given in Å. The values were calculated using the COMPSTRU structure utility provided by the Bilbao crystallographic server.[39]

WP	Atom	Atomic displacements				
		u_x	u_y	u_z	$\|\|u\|\|$	
18f	Ge1	−0.0035	−0.0072	0.0021	0.0910	XRD
		−0.0017	−0.0010	0.0031	0.0366	PBE
		−0.0017	−0.0007	0.0030	0.0356	HSE06
18f	Zn1	0.0007	−0.0006	−0.0021	0.0256	XRD
		−0.0033	−0.0001	−0.0014	0.0477	PBE
		−0.0039	0.0002	−0.0012	0.0577	HSE06
18f	Zn2	0.0019	0.0105	0.0036	0.1421	XRD
		−0.0009	0.0048	0.0027	0.0796	PBE
		−0.0010	0.0048	0.0026	0.0798	HSE06
18f	O1	−0.0075	−0.0001	−0.0041	0.1130	XRD
		−0.0014	0.0002	0.0061	0.0622	PBE
		−0.0015	0.0006	0.0070	0.0715	HSE06
18f	O2	0.0246	0.0082	0.0273	0.4038	XRD
		0.0031	0.0033	0.0062	0.0744	PBE
		0.0032	0.0042	0.0054	0.0745	HSE06
18f	O3	−0.0145	−0.0119	−0.0162	0.2453	XRD
		−0.0027	0.0005	0.0023	0.0478	PBE
		−0.0029	−0.0001	0.0021	0.0450	HSE06
18f	O4	0.0019	−0.0013	−0.0024	0.0458	XRD
		0.0003	−0.0024	−0.0077	0.0450	PBE
		−0.0001	−0.0030	−0.0084	0.0910	HSE06

freely in order to test for potential atom site hopping. Neither the Ge1 (0.97(2)), nor the Zn1 (1.00(3)) site occupancies differ significantly from unity and it is hence expected that no significant cation permutation occurs. Interestingly, the second independent Zn position (Zn2) exhibits a sub-stoichiometric occupancy of 0.92(3). This cannot be explained with a mixed occupation with Ge, since the Ge scattering length is larger than the one for Zn. Instead, this must be an effect of a Zn deficit, which coincides with traces of unreacted ZnO in the final product. It is, nonetheless, interesting that the willemite structure remains intact despite of the sub-stoichiometry. Further, there is no distinct hint in the valences of the different sites as calculated using Bond valence sums (Figure 4).[31] Instead, the valences around Zn1 sum to 2.042, around Zn2 to 2.075 and around Ge1 to 3.896. They are, hence, close to the charge of the respective ions and do not give rise to concern.

DFT Studies

The experimental investigation of the structural properties of willemite-type Zn_2GeO_4 is supplemented by a DFT investigation utilizing the standard GGA approximation in the PBE parametrization[32] and the more accurate hybrid functional HSE06,[33,34] as outlined in the computational details section. For both functionals, several fixed-volume calculations have been performed around the experimental ground state volume, allowing the internal structural parameters to fully relax. The obtained total energy curves have then been fitted to Murnaghan's equation of state:[35,36]

$$E(V) = E(V_0) + \frac{B_0\, V}{B'_0}\left[\frac{\left(\frac{V_0}{V}\right)^{B'_0}}{B'_0 - 1} + 1\right] - \frac{V_0 B_0}{B'_0 - 1}$$

to determine the ground-state volume V_0, the bulk modulus B_0, and its pressure derivative B'_0, respectively.

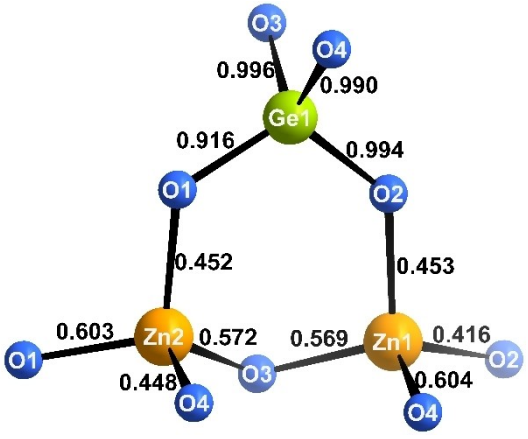

Figure 4. The bond valences v_{ij} of the Zn–O and Ge–O bonds in Zn_2GeO_4 as refined from neutron diffraction.

The obtained structural properties are given together with the experimental results in Table 1. It can be seen that the calculated unit cells are 4.9% and 1.6% larger compared to the experimental values for the PBE and HSE06 levels of theory, respectively. This is mostly due to the well-known overbinding at the PBE level of theory, improves significantly when switching to the more accurate hybrid functional HSE06, and has been observed for other oxide semiconductors before.[37,38] The bulk modulus B_0 and its pressure derivative B'_0 are 106.4 GPa (117.3 GPa) and 2.6 (2.1) at the PBE (HSE06) level of theory, and are in fair agreement to experimental results of 117.8 GPa and 4[27] and 151.7 GPa and 4,[12] respectively.

A closer look at the fractional atomic coordinates obtained at the PBE (HSE06) level of theory, as given in the supplementary Tables S7 (S9), reveals that they only differ around the third digit. Given the better agreement of the HSE06 ground state volume with the experimental results from X-ray and neutron refinement, a detailed comparison to the experimental atom positions will be restricted to the HSE06 structure only. Taking the atomic positions refined from neutron diffraction as reference values, Table 2 shows the comparison to the atomic positions refined from X-ray diffraction and calculated at the PBE and HSE06 level of theory, obtained from the COMPSTRU structure utility provided by the Bilbao crystallographic server.[39] With the exception of Zn1, the cation positions of both, PBE and HSE06 structure optimizations, are in better agreement with the atomic positions obtained from neutron diffraction compared to the atomic positions obtained from X-ray diffraction. The agreement between theory and neutron diffraction is also better compared to taking the atomic positions from X-ray diffraction as reference values, as given in supplementary Table S11. The agreement between neutron diffraction data and DFT calculations further underlines a high level of confidence in the results obtained and hence supports the experimental part of this study greatly.

For the oxygen positions, with the exception of O4, the agreement between neutron diffraction and theory is much better compared to X-ray diffraction. This is seemingly in contrast to a very good agreement of the O4 atomic positions from theory compared to X-ray diffraction, as given in supplementary table S11. One remarkable feature is the position of O4, where the discrepancy between calculated and refined position is primarily along the crystallographic *c*-axis. This behavior can be related to the structural features of this particular oxygen site. All oxygen sites are coordinated in a nearly trigonal planar manner, but while the trigonal planes for O1–O3 are oriented parallel to the *c*-axis, the trigonal plane for O4 is perpendicular to the *c*-axis. Therefore, this discrepancy may be sign of a higher degree of motional freedom of this oxygen position and might be taken as a hint for potential increased oxygen ion conductivity at higher temperatures. It should be noted, however, that unlike this geometrical argument, O2 exhibits the largest displacement parameters and hence has the highest degree of motional freedom. This is in line with the bond valence sum for O2 (1.863), which is smaller than those of O1 (1.971), O3 (2.137) and O4 (2.042) and smaller than the expected value of 2 (compare Figure 4). This can be

taken as indicator for a weaker bonding environment for O2 and hence increased thermal motion. The electronic band structure of willemite-type Zn_2GeO_4 is given in Figure 5. While the shaded gray area depicts the electronic properties calculated with the simpler PBE functional, the valence (green) and conduction bands (red) are calculated with the more accurate HSE06 functional, respectively. The electronic band gap is direct and located at the center of the Brillouin zone, and amounts to 1.944 eV (4.006 eV) utilizing the PBE (HSE06) functionals. While the PBE band gap of 1.944 eV is strongly underestimated with respect to the experimental band gap of 4.4 eV,[4] the HSE06 band gap of 4.006 eV is in much better agreement. This is in line with the general trend that hybrid functional calculations for oxide semiconductors yield better agreement of lattice parameters and band gaps with respect to experimental results.[37]

Apart from a detailed investigation of the structural properties of willemite-type Zn_2GeO_4, we were also interested in possible cation permutations. To this end, we performed additional Γ-point only calculations based on a 2×2×2 supercell of the relaxed ground state structure, now containing 336 atoms or 48 f.u. of Zn_2GeO_4. Of the possible cation permutations in willemite-type Zn_2GeO_4 between Zn and Ge cations, we considered the ones between the unique Ge1 and the two different Zn1 and Zn2 positions, respectively. The structures of both defective supercells, namely Zn1-Ge1 and Zn2-Ge1, have been relaxed until the forces on all the atoms were below 0.01 eV Å^{-1}. The obtained energy differences are +55 meV (+63 meV) per f.u. of Zn_2GeO_4 for the Zn1-Ge1 and +52 meV (+60 meV) for the Zn2-Ge1 antisite defect, calculated at the PBE (HSE06) level of theory, respectively. Since the synthesis temperature was chosen as 1100 °C (1373 K), it is reasonable to assume that the thermal energy of the synthesis conditions would be sufficient to relax the system into the thermodynamically favored, ordered state.

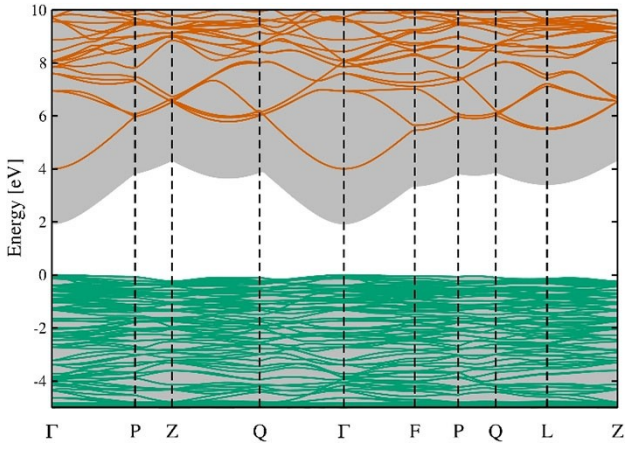

Figure 5. Electronic band structure of willemite-type Zn_2GeO_4. Valence (green) and conduction bands (red) are calculated with the HSE06 functional, whereas the shaded gray area depicts the results for the PBE functional. Energies are in electron volt (eV) with the valence band maximum set to zero.

Conclusions

Using a combination of X-ray and neutron powder diffraction, we re-determined the crystal structure of Zn_2GeO_4 at ambient conditions. The crystal structure was unambiguously confirmed as willemite-type structure with tetrahedrally coordinated cations. Supplementing the neutron diffraction with DFT calculations based on the PBE and the more accurate hybrid functional HSE06, we further confirmed the cation ordering that is not directly accessible through X-ray diffraction. While the great positional degree of freedom in the willemite type – all atoms lie on general positions – would allow for cation permutation disorder, no such effect has been observed herein. The results from neutron diffraction compare excellently with the simulated atomic positions from DFT calculations and, therefore, add a further level of confidence. Additional DFT calculations on 2×2×2 supercells containing two possible cation permutations revealed that the thermal barriers are in the range of the applied synthesis temperatures. We therefore do not expect any significant cation permutations to be present in our samples and conclude that, the presently chosen synthesis conditions are sufficient to relax the system into the ordered state.

Experimental Section

Synthesis and experimental characterization

Zn_2GeO_4 was synthesized in a procedure adapted from Viennois et al.,[13] from the respective oxides ZnO (99%, Fisher Scientific) and GeO_2 (99.999%, ACROS Organics). The oxides were mixed in the stoichiometric 2:1 ratio and ground in an agate mortar. The mixture was then pressed into pellets and heated to 1100 °C with a ramp of 200 K/h, where it was held for 72 hours in a box furnace in air. The furnace was then allowed to cool to room temperature naturally. X-ray diffraction patterns were recorded using a Bruker d8 Advance system with Ni-filtered Cu–Kα radiation and a LynxEye detector. LaB_6 was added as internal standard for the measurements. Neutron diffraction was recorded on the fine resolution powder diffractometer (E9)[40] at the BERII neutron source with Ge(511) monochromatized neutron beam at a wavelength of 1.7982 Å. The data was refined using the published crystal structure of willemite-type Zn_2GeO_4 as starting model[21] and using Jana2006.[41] Further details of the refinement procedure are given in the results section.

Computational details

The DFT calculations were performed using the Vienna ab initio simulation package (VASP 5.4.4)[42–44] together with the projector-augmented wave (PAW) method.[45,46] The calculations were performed with the generalised gradient approximation (GGA) in the parametrization of Perdew, Burke, and Ernzerhof (PBE)[32] and the hybrid functional HSE06.[33,34] PAW potentials supplied with the VASP package were used and contributed 12, 14 and 6 valence electrons for the Zn ($3d^{10}$ $4s^2$), Ge ($3d^{10}$ $4s^2$ $4p^2$), and O ($2s^2$ $2p^4$) atoms, respectively. Structural relaxations were performed for the rhombohedral unit cell containing 42 atoms, that is 6 formula units (f.u.) of Zn_2GeO_4, until the forces on all atoms were below 0.005 eV Å^{-1}. Together with a *k*-point grid of 6×6×6 (4×4×4) for

the PBE (HSE06) calculations, a cut-off energy of 500 eV and the convergence criteria for the energy of 10^{-5} eV this ensured well-converged results.

Acknowledgements

The authors thank Albina Glibo for assistance with synthesis. This work made use of computational resources provided by the North-German Supercomputing Alliance (HLRN, www.hlrn.de), and the Dirac and Curta HPC facilities[47] of the Helmholtz-Zentrum Berlin and the Freie Universität Berlin, respectively. Helmholtz-Zentrum Berlin is acknowledged for use of the diffractometer E9 at the BER-II research reactor under proposal number 18106681-EF. Open Access funding enabled and organized by Projekt DEAL.

Conflict of Interest

The authors declare no conflict of interest.

Keywords: neutron diffraction · ab initio calculation · ternary oxide · crystal structure

[1] R. Yi, J. Feng, D. Lv, M. L. Gordin, S. Chen, D. Choi, D. Wang, *Nano Energy* **2013**, *2*, 498–504.
[2] F. Zou, X. Hu, L. Qie, Y. Jiang, X. Xiong, Y. Qiao, Y. Huang, *Nanoscale* **2014**, *6*, 924–930.
[3] X. Li, Y. Feng, M. Li, W. Li, H. Wei, D. Song, *Adv. Funct. Mater.* **2015**, *25*, 6858–6866.
[4] Z. Liu, X. Jing, L. Wang, *J. Electrochem. Soc.* **2007**, *154*, H500.
[5] S. Wu, Z. Wang, X. Ouyang, Z. Lin, *Nanoscale* **2013**, *5*, 12335–12341.
[6] M. Shang, G. Li, D. Yang, X. Kang, C. Peng, Z. Cheng, J. Lin, *Dalton Trans.* **2011**, *40*, 9379–9387.
[7] G. Gao, L. Wondraczek, *J. Mater. Chem. C* **2013**, *1*, 1952–1958.
[8] S. Zhang, Y. Hu, R. Chen, X. Wang, Z. Wang, *Opt. Mater.* **2014**, *36*, 1830–1835.
[9] Q. Liu, Y. Zhou, J. Kou, X. Chen, Z. Tian, J. Gao, S. Yan, Z. Zou, *J. Am. Chem. Soc.* **2010**, *132*, 14385–14387.
[10] N. Zhang, S. Ouyang, P. Li, Y. Zhang, G. Xi, T. Kako, J. Ye, *Chem. Commun.* **2011**, *47*, 2041–2043.
[11] R. Stevens, B. F. Woodfield, J. Boerio-Goates, M. K. Crawford, *J. Chem. Thermodyn.* **2004**, *36*, 349–357.
[12] X. Cheng, J. Yuan, X. Zhu, K. Yang, M. Liu, Z. Qi, *J. Phys. D* **2018**, *51*, 095303.
[13] R. Viennois, T. Taliercio, V. Potin, A. Errebbahi, B. Gil, S. Charar, A. Haidoux, J.-C. Tédenac, *Mater. Sci. Eng. B* **2001**, *82*, 45–49.
[14] J. Huang, Y. Cui, X. Wang, *Environ. Sci. Technol.* **2010**, *44*, 3500–3504.
[15] N. Zhang, S. Ouyang, T. Kako, J. Ye, *Chem. Commun.* **2012**, *48*, 1269–1271.
[16] J. Breternitz, Z. Wang, A. Glibo, A. Franz, M. Tovar, S. Berendts, M. Lerch, S. Schorr, *Phys. Status Solidi A* **2019**, *216*, 1800885.
[17] N. C. Coronel, L. Lahourcade, K. T. Delaney, A. M. Shing, H. A. Atwater, *38th IEEE Photovoltaics Specialists Conference*, **2012**.
[18] A. Punya, W. R. L. Lambrecht, *Phys. Rev. B* **2013**, *88*, 075302.
[19] F. Tessier, P. Maillard, Y. Lee, C. Bleugat, K. Domen, *J. Phys. Chem. C* **2009**, *113*, 8526–8531.
[20] C. Hang, M. A. Simonov, N. V. Belov, *Kristallografiya* **1970**, *15*, 457.
[21] A. Oribe, K. Tanaka, H. Morikawa, F. Marumo, *Report of the Research Laboratory on Engineering Materials*, p.7. Tokyo, Japan, Tokyo Institute of Technology.
[22] W. L. Bragg, W. H. Zachariasen, *Z. Kristallogr.* **1930**, *72*, 518–528.
[23] F. Hund, *Z. Anorg. Allg. Chem.* **1970**, *374*, 191.
[24] K.-H. Klaska, J. C. Eck, D. Pohl, *Acta Crystallogr. Sect. B* **1978**, *34*, 3324–3325.
[25] M. Kanzaki, *J. Mineral. Petrol. Sci.* **2018**, *113*, 41–46.
[26] Q. Bai, Z. Wang, P. Li, S. Xu, T. Li, J. Cheng, Z. Yang, *Mater. Des.* **2016**, *108*, 597–607.
[27] S.-W. Yang, F. Peng, W.-T. Li, Q.-W. Hu, X.-Z. Yan, L. Lei, X.-D. Li, D.-W. He, *Chin. Phys. B* **2016**, *25*, 076101.
[28] R. D. Shannon, *Acta Crystallogr. Sect. A* **1976**, *32*, 751–767.
[29] M. Henry, *Coord. Chem. Rev.* **1998**, *178–180*, 1109–1163.
[30] V. F. Sears, *Neutron News* **1992**, *3*, 26–37.
[31] N. E. Brese, M. O'Keeffe, *Acta Crystallogr. Sect. B* **1991**, *47*, 192–197.
[32] J. P. Perdew, K. Burke, M. Ernzerhof, *Phys. Rev. Lett.* **1996**, *77*, 3865–3868.
[33] J. Heyd, G. E. Scuseria, M. Ernzerhof, *J. Chem. Phys.* **2003**, *118*, 8207–8215.
[34] J. Heyd, G. E. Scuseria, M. Ernzerhof, *J. Chem. Phys.* **2006**, *124*, 219906.
[35] F. D. Murnaghan, *Amer. J. Math.* **1937**, *59*, 235–260.
[36] F. D. Murnaghan, *Proc. Natl. Acad. Sci. USA* **1944**, *30*, 244–247.
[37] D. Fritsch, B. J. Morgan, A. Walsh, *Nanoscale Res. Lett.* **2017**, *12*, 19.
[38] D. Fritsch, *In Theory and Simulation in Physics for Materials Applications: Cutting-Edge Techniques in Theoretical and Computational Materials Science*, edited by E. V. Levchenko, Y. L. Dappe & G. Ori, p. 79. Springer.
[39] G. de la Flor, D. Orobengoa, E. Tasci, J. M. Perez-Mato, M. I. Aroyo, *J. Appl. Crystallogr.* **2016**, *49*, 653–664.
[40] A. Franz, A. Hoser, *J. Large-Scale Res. Fac.* **2017**, *3*, A103.
[41] V. Petříček, M. Dušek, L. Palatinus, *Z. Kristallogr. Cryst. Mater.* **2014**, *229*, 345–352.
[42] G. Kresse, J. Hafner, *Phys. Rev. B* **1993**, *47*, 558–561.
[43] G. Kresse, J. Hafner, *Phys. Rev. B* **1994**, *49*, 14251–14269.
[44] G. Kresse, J. Furthmüller, *Comp. Mat. Sci.* **1996**, *6*, 15–50.
[45] P. E. Blöchl, *Phys. Rev. B* **1994**, *50*, 17953–17979.
[46] G. Kresse, D. Joubert, *Phys. Rev. B* **1999**, *59*, 1758–1775.
[47] L. Bennett, B. Melchers, and B. Proppe, *Curta: A general-purpose high-performance computer at ZEDAT*, Freie Universität Berlin (2020). doi: 10.17169/refubium-26754.

Manuscript received: July 15, 2021
Revised manuscript received: October 7, 2021

